Biochimica et Biophysica Acta 1827 (2013) 914–922

Contents lists available at SciVerse ScienceDirect

Biochimica et Biophysica Acta

journal homepage: www.elsevier.com/locate/bbabio

Review

Influence of protein interactions on oxidation/reduction midpoint potentials of cofactors in natural and de novo metalloproteins ☆

T.L. Olson, J.C. Williams, J.P. Allen *

Department of Chemistry and Biochemistry, Arizona State University, Tempe AZ 85287-1604, USA

ARTICLE INFO

Article history:
Received 3 December 2012
Received in revised form 13 February 2013
Accepted 23 February 2013
Available online 4 March 2013

Keywords:
Photosynthesis
Cytochrome
Bacteriochlorophyll
Manganese cofactor
Reaction center
Photosystem II

ABSTRACT

As discussed throughout this special issue, oxidation and reduction reactions play critical roles in the function of many organisms. In photosynthetic organisms, the conversion of light energy drives oxidation and reduction reactions through the transfer of electrons and protons in order to create energy-rich compounds. These reactions occur in proteins such as cytochrome *c*, a heme-containing water-soluble protein, the bacteriochlorophyll-containing reaction center, and photosystem II where water is oxidized at the manganese cluster. A critical measure describing the ability of cofactors in proteins to participate in such reactions is the oxidation/reduction midpoint potential. In this review, the basic concepts of oxidation/reduction reactions are reviewed with a summary of the experimental approaches used to measure the midpoint potential of metal cofactors. For cofactors in proteins, the midpoint potential not only depends upon the specific chemical characteristics of cofactors but also upon interactions with the surrounding protein, such as the nature of the coordinating ligands and protein environment. These interactions can be tailored to optimize an oxidation/reduction reaction carried out by the protein. As examples, the midpoint potentials of hemes in cytochromes, bacteriochlorophylls in reaction centers, and the manganese cluster of photosystem II are discussed with an emphasis on the influence that protein interactions have on these potentials. This article is part of a Special Issue entitled: Metals in Bioenergetics and Biomimetics Systems.

1. Introduction

In photosynthesis, oxidation/reduction (redox) reactions involving pigment-protein complexes play key roles in the conversion of light energy into chemical energy. In anoxygenic photosynthetic bacteria such as *Rhodobacter sphaeroides*, light energy is initially absorbed by antenna complexes followed by energy transfer to the reaction center, where the primary photochemistry occurs [1,2]. The energy transfer results in excitation of the bacteriochlorophyll (BChl) dimer termed P865, which is followed by a series of redox reactions involving the excited state of P865 (P865*) serving as the primary electron donor and a series of electron acceptors, a bacteriochlorophyll monomer, bacteriopheophytin monomer, the primary quinone, and the secondary quinone (Q_B). After a water-soluble cytochrome c_2 reduces the oxidized bacteriochlorophyll dimer ($P865^{\bullet+}$), a second electron can be transferred to Q_B in a proton-coupled redox process that generates a quinol. The quinol carries the electrons and protons to the cytochrome bc_1 complex in a redox cycle that generates the proton gradients needed for the creation of energy-rich compounds.

In oxygenic photosynthesis, two pigment-protein complexes, photosystem I and II, participate in the Z scheme, which has terminal electron donors and acceptors rather than operating in the cyclic process found in bacteria [3]. In this scheme, light excitation of photosystem II results in oxidation of the primary electron donor (P680) that is reduced by a redox active tyrosine (Y_Z) in a proton-coupled redox reaction. The tyrosyl is then reduced by the site of water oxidation, namely the Mn_4Ca cluster. After four photons of light have been absorbed and four electrons have been transferred, two water molecules bound to the Mn_4Ca cluster are converted into molecular oxygen. The use of water as an electron donor in this four-electron, four-proton redox reaction requires that cofactors be highly oxidizing, making P680 the strongest known oxidant in nature.

In order to have the light-driven redox reactions proceed with a quantum efficiency of near unity in photosynthetic complexes, electron transfer in the forward reactions must be very favorable, and any side reactions and undesired back reactions must be minimized. Theoretical treatments have identified the electron transfer parameters that the protein surrounding the cofactors of the reaction center can alter, namely the energetics, the coupling, and the protein dynamics [4]. Key to maintaining a balance between favorable and unfavorable reactions is the fine-tuning of the redox potentials of the electron acceptors and donors through interactions with the protein in which they are embedded.

This paper will review how specific interactions can alter the energetics of cofactors, in particular the redox midpoint potentials.

☆ This article is part of a Special Issue entitled: Metals in Bioenergetics and Biomimetics Systems.

* Corresponding author. Tel.: +1 480 965 8241; fax: +1 480 965 2747.
E-mail address: jallen@asu.edu (J.P. Allen).

0005-2728/$ – see front matter © 2013 Elsevier B.V. All rights reserved.
http://dx.doi.org/10.1016/j.bbabio.2013.02.014

Initially the basic concepts of redox reactions are presented, including a definition of a redox midpoint potential, followed by a short discussion of the experimental approaches used to determine midpoint potentials. Examples are then presented for three types of cofactors. The potentials of hemes are discussed with an emphasis on lessons learned from cytochromes and *de novo* proteins, followed by BChls, with an emphasis on how both pigment and protein interactions influence the energetics of cofactors. Finally, the energetics of manganese cofactors, ranging from mononuclear cofactors as found in superoxide dismutase to the Mn_4Ca cluster of photosystem II, are presented, with a focus on the factors that contribute to the highly oxidizing nature of the cofactors of photosystem II.

2. Redox reactions

Redox reactions can be considered to involve a redox couple, namely the reduced and oxidized states of a molecule, A_{red} and A_{ox} respectively, that are part of a reaction resulting in the transfer of n electrons:

$$A_{red} \leftrightarrow A_{ox} + ne^- \tag{1}$$

For this reaction, the change in the Gibbs energy, ΔG, is given by the sum of the standard Gibbs energy, $\Delta G°$, and the natural log of the equilibrium constant, K_{eq}, that can be expressed in terms of the relative concentrations of the oxidized and reduced molecules:

$$\Delta G = \Delta G° + RT \ln K_{eq} = \Delta G° + RT \ln \frac{[A_{ox}]}{[A_{red}]} \tag{2}$$

where R is the gas constant and T is the temperature. For a reaction that proceeds forward, the change in the Gibbs energy, sometimes termed the driving force, is negative. Since redox experiments measure the transfer of electrons through electrical measurements, energies are typically described in terms of voltages rather than Gibbs energies. The change in potential, ΔE, is related to the change in Gibbs energy by the Faraday constant, F, and n according to:

$$\Delta E = -\Delta G \Big/ nF \tag{3}$$

The reference potential is usually chosen to be the standard hydrogen cell that is assigned the value of 0 V resulting in the expression:

$$E = E_m + \frac{RT}{nF} \ln \frac{[A_{ox}]}{[A_{red}]} \tag{4}$$

where E_m represents the midpoint potential, that is, the potential at which $[A_{ox}]$ equals $[A_{red}]$. Since many redox couples behave as weak acids or bases, the midpoint potentials can be pH dependent. In the strongly-coupled limit, E_m is dependent upon pH according to:

$$E_m(pH) = E° - \frac{0.0591\ V}{n}\ pH \tag{5}$$

where $E°$ is the standard half-reduction potential (pH = 0). For a one-electron redox reaction as observed for a biological protein such as a cytochrome, the E_m value would decrease by approximately 0.06 V for each pH unit. In cases where the coupling is weak, the pH dependence is reduced. For example the primary electron donor P865 is buried within the bacterial reaction center, and the P865/P865$^{\bullet+}$ midpoint potential, E_m(P865/P865$^{\bullet+}$), has a weak dependence upon pH, with the potential decreasing by only 0.02 V as the pH increases from 6.0 to 9.5 [5–7].

If there is a second molecule that undergoes the opposite process, namely becoming reduced, the overall reaction is:

$$A_{red} + B_{ox} \leftrightarrow A_{ox} + B_{red} \tag{6}$$

where the electrons are not explicitly included as they are balanced in the overall equation. For this reaction the overall change in the potential is given by the Nernst equation:

$$E = E° + \frac{RT}{nF} \ln \frac{[A_{ox}][B_{red}]}{[A_{red}][B_{ox}]} \tag{7}$$

The overall reaction can be divided into two half reactions, one for the oxidation of A and the other for the reduction of B. Knowing the potentials associated with each of the individual half reactions allows the overall energetic changes for the full reaction to be determined since the terms are additive. Thus, E_m represents a simple parameter that can be used to understand redox reactions.

The chemical nature of the cofactor is the primary determinant of E_m but interactions with the surrounding protein can significantly alter the potential. The nature of the coordinating ligands of metal cofactors can play a critical role because of their direct impact on the electronic structure. Hydrogen bonds to the conjugated tetrapyrroles of BChls and Chls also influence the energies of the valence electrons that are removed upon oxidation. Electrostatic interactions with ionizable amino acid residues will shift E_m, for example positively-charged amino acid residues make oxidation of cofactors more difficult and thus increase E_m. Several nearby charged residues may influence E_m for a cofactor, although the electrostatic contribution of individual residues can be identified through theoretical calculations, as has been done for different cofactors including P865, P680, and the hemes in the tetraheme subunit of reaction centers [8–10]. Electrostatic interactions are modulated by the dielectric constant, with small values of the dielectric constant in the hydrophobic interiors of proteins increasing the strength of the interactions and hence the impact on E_m compared to more polar environments. The values of the dielectric constant within a protein can be inhomogeneous because of their nonuniform nature. In addition, for proteins with multiple cofactors, including the complexes discussed in this review, interactions between cofactors can influence the midpoint potentials. The midpoint potential of each cofactor may be dependent upon the redox states of the surrounding cofactors, which change as electron transfer occurs between the cofactors [11]. Below, we first briefly summarize some methodologies used to determine E_m and then discuss in detail how such interactions between cofactors and the protein environment modify E_m. Hemes, BChls and Chls, and Mn-cofactors, which are common electron transfer cofactors, are presented as examples.

2.1. Experimental determination of midpoint potentials

While the midpoint potentials of metal cofactors of small redox proteins can be determined using cyclic voltammetry, for larger proteins, such as Mn-superoxide dismutase and reaction centers, the cofactors are slow to equilibrate with the external potential making such measurements difficult [12–14]. Instead, the midpoint potential of a metal cofactor is typically measured experimentally using either a chemical or electrochemical titration of the protein, in which the relative amount of the reduced and oxidized species at each potential is determined [15,16]. The measurements must be reversible to be thermodynamically viable, and so care must be taken to avoid extreme potentials in order to avoid denaturation of the protein. When done chemically, the titrations involve chemical oxidants and reductants, such as ferri/ferrocyanide mixtures. One disadvantage of such measurements is a constant dilution of the sample as the oxidizing and reducing agents are added. For the electrochemical titrations the samples are sealed and the potentials are poised by the use of electrodes. In both cases, the easiest manner to determine the relative amount of oxidized and reduced species is to monitor an optical absorption transition associated with the cofactor. For example, reduced hemes of cytochrome typically have strong absorption bands in the 500–600 nm region but only a broad, weak absorption band when

oxidized. If such optical measurements are being performed with chemical titrations then typically the protein solution is pumped between a mixing chamber and an optical cuvette. For electrochemical cells, the electrodes are placed into a cell with a short optical pathlength, thus requiring concentrated samples for accurate measurements of the absorption changes. In order to ensure electrical equilibrium in both cases, the solutions must contain mediators and electrolytes that act reversibly and are chemically inert to the proteins. Mediators are chosen that have a midpoint potential suitable for the range of measurements, for example, diaminodurol and benzylviologen have potentials of +0.22 V and −0.3 V, respectively [16]. If a large range of potentials is being swept during the measurements, then a mixture of mediators are utilized with overlapping potential regions.

If a cofactor does not have a clear spectroscopic signal, direct measurements of the midpoint potential are not viable. For an electron transfer reaction between an electron donor and acceptor, both the rate of the reaction and the relative yield are dependent upon the free energy difference, which is determined by the relative values of the midpoint potentials of the donor and acceptor (Eq. (3)). Thus, the midpoint potential can be estimated by measurement of either the rate or the equilibrium concentrations. For photosystem II, such indirect measurements have been used to estimate the potentials of P680, Y_Z, and the Mn_4Ca cluster [17–20]. A specific example of an indirect measurement based upon equilibrium concentrations is given below where the midpoint potential of the Mn-cofactor of modified reaction centers is determined by monitoring the oxidation state of P865.

2.2. Midpoint potentials of hemes

Hemes are porphyrins with a central iron coordinated by four planar nitrogens and typically two axial ligands from amino acid side chains. Reduction of another protein by cytochrome results in a change from the Fe^{2+} to the Fe^{3+} state, likewise oxidation by cytochrome results in the change from Fe^{3+} to Fe^{2+}. Thus, the redox properties, as determined by the midpoint potential of the heme iron, $E_m(Fe^{2+}/Fe^{3+})$, are a critical factor in the biological roles of cytochromes. Hemes can have different chemical substitutents as denoted by the different classes of types *a*, *b*, *c*, and *d*. Each type of heme has a different intrinsic $E_m(Fe^{2+}/Fe^{3+})$, for example the potentials of *b*-type hemes are typically 0.4 V lower than observed for *a*-type hemes [21,22].

Extensive studies have provided a wealth of midpoint potential data for cytochromes showing that hemes can operate in proteins over a wide range of potentials. A variety of studies have shown that the potential is strongly influenced by the identity of the two axial ligands to the central iron. In general, more basic ligands are better electron donors and thus preferentially stabilize the Fe^{3+} state and decrease the $E_m(Fe^{2+}/Fe^{3+})$ value. For example, the central heme iron in *c*-type cytochromes is typically coordinated by Met and His axial ligands (Fig. 1) [23,24]. These hemes usually have a $E_m(Fe^{2+}/Fe^{3+})$ of ~0.3 V, with substitutions to a variety of different ligands, including thiol groups and non-natural ligands, changing the potential by up to 0.4 V [25]. Computational studies of cytochromes estimate that replacement of the Met ligand with His lowers the potential by 0.2 V [26]. Electrostatic interactions between solvent-exposed hemes and the surrounding ions in solution give rise to a pronounced dependence on pH (Eq. (5)) that is dependent upon the extent of screening by the intervening protein [21].

These types of protein interactions are balanced in cytochromes in order to poise the operating $E_m(Fe^{2+}/Fe^{3+})$ such that it can perform the needed electron transfer reactions in the cell. For example, cytochrome c_2 from *Rb. sphaeroides* serves as an electron carrier between the bacterial reaction center and the cytochrome bc_1 complex. The $E_m(Fe^{2+}/Fe^{3+})$ value of 0.35 V for cytochrome c_2 is positioned between the potentials of 0.29 V for the c_1 heme of cytochrome bc_1 and 0.505 V for P865 of the reaction center [4,15,27,28], allowing the cytochrome c_2 to serve as an electron acceptor from the cytochrome bc_1 complex and an electron donor to the reaction center.

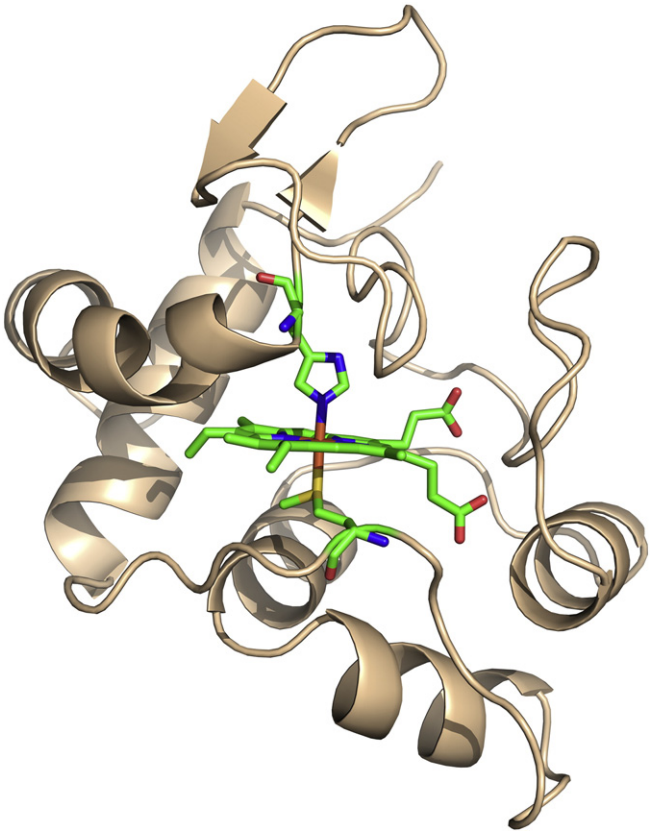

Fig. 1. Three-dimensional structure of cytochrome c_2 from *Rb. sphaeroides*. The structure shows the overall globular fold of the alpha helices (wheat) surrounding the heme cofactor (colored by atom type) whose central iron is coordinated by two axial ligands, His 19 and Met 100. Coordinates described in Axelrod and coworkers [24] (1CXC).

In many purple bacteria, the BChl dimer is reduced by a bound tetraheme cytochrome subunit that is subsequently reduced by a cytochrome c_2 [29]. The tetraheme cytochrome of *Blastochloris viridis* consists of 336 amino acid residues forming short alpha helices that surround four covalently linked hemes [30] (Fig. 2). The protein subunit and the hemes break the approximate two-fold symmetry of the reaction center and are inclined approximately 30° relative to the membrane normal. The four hemes can be spectrally distinguished, allowing electrochemical determination of the $E_m(Fe^{2+}/Fe^{3+})$ of the individual hemes whose $E_m(Fe^{2+}/Fe^{3+})$ values range from −0.06 V to +0.38 V in *Bl. viridis* [31,32]. The coordination of the individual hemes partially determines $E_m(Fe^{2+}/Fe^{3+})$, as the heme with one of the low potentials has two His ligands. The other three hemes all have His and Met ligands but significantly different potentials showing that other protein interactions also play a role in establishing $E_m(Fe^{2+}/Fe^{3+})$. The contributions of the protein interactions have been incorporated into computational models that have correctly assigned the potentials of the four hemes within the tetraheme cytochrome of *Bl. viridis* [8]. An outcome of these computational studies is that the observed differences in potentials reflect an inhomogeneity of the effective dielectric constant in the protein, and heme-heme interactions, in addition to a few specific interactions between amino acid side chains and the hemes.

The incorporation of hemes into *de novo* proteins has proven to serve as a useful framework for the design of catalytic proteins [33–37]. The four-helix bundle motif provides a large interface between

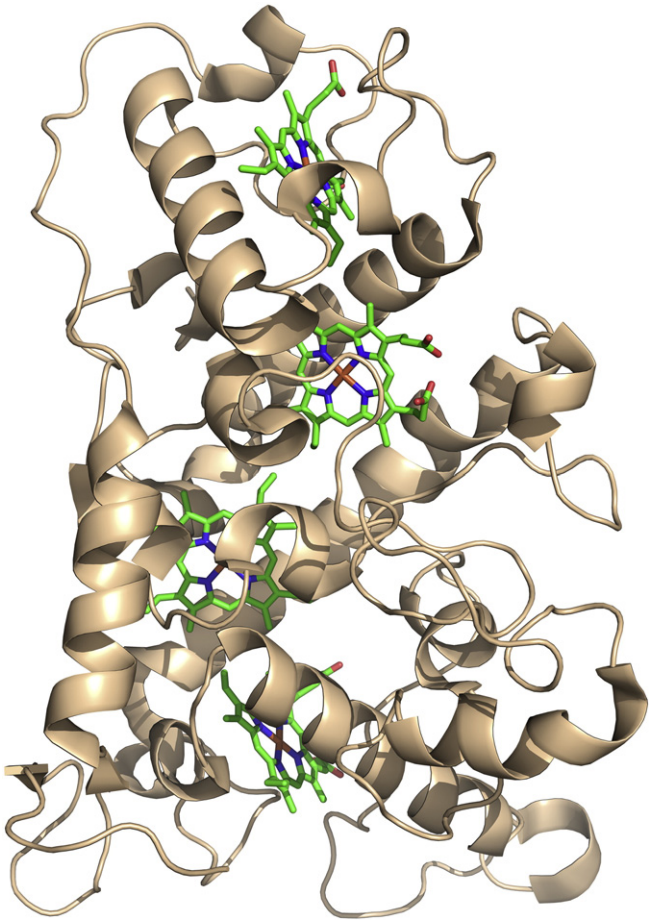

Fig. 2. Three-dimensional structure of the tetraheme cytochrome from *Bl. viridis*. The structure shows the overall globular fold of the alpha helices (wheat) surrounding four heme cofactors (colored by atom type). The heme at the bottom center of the figure is the closest to the bacteriochlorophyll dimer and serves as the secondary electron donor. Coordinates described in Deisenhofer and coworkers [30] (1PRC).

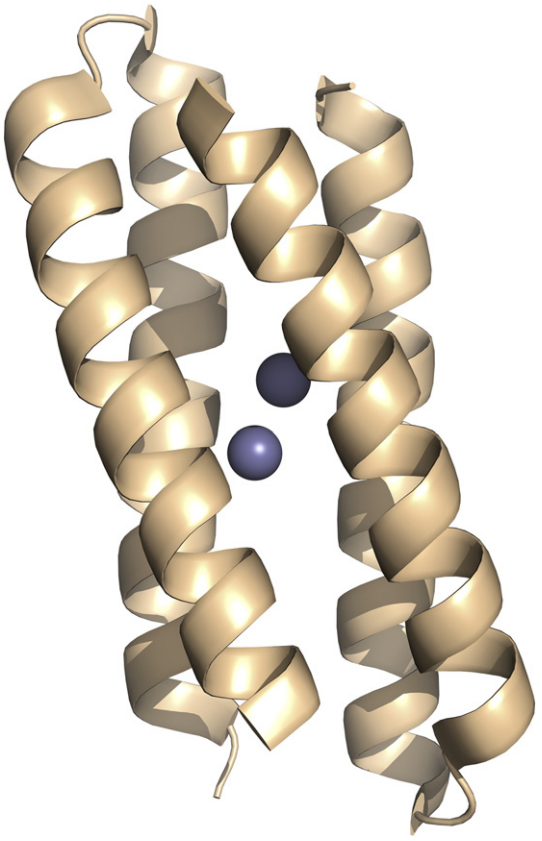

Fig. 3. Three-dimensional structure of a *de novo* four-helix bundle. The structure shows two subunits (wheat) each of which has two long helices surrounding a central dinuclear Zn cofactor (purple). Coordinates from Lahr and coworkers [38] (1MFT).

subunits for the incorporation of cofactors held by suitable ligands, with the incorporation of a dinuclear Zn cofactor producing a stable structure that was solved by X-ray diffraction [38] (Fig. 3). These *de novo* designed proteins are providing a re-examination of the interactions that establish the redox properties of hemes in protein environments. Most of the designs utilize a four-helix bundle and a heme *b* that has an intrinsic $E_m(Fe^{2+}/Fe^{3+})$ of −0.235 V with two His axial ligands. The use of other ligands including unnatural amino acids has been investigated, for example, two pyridines serving as axial ligands raised $E_m(Fe^{2+}/Fe^{3+})$ to +0.6 V [39]. Changes in other protein interactions, such as electrostatic interactions with polar residues, generally changed the potential by up to 0.2 V, and the $E_m(Fe^{2+}/Fe^{3+})$ has been found to have a sharp pH dependence (Eq. (5)) [40]. Designs have also investigated the roles of detergents and membranes in the properties of cofactors, for example a $E_m(Fe^{2+}/Fe^{3+})$ of −0.13 V was observed for the heme *b* bound to a *de novo* designed model of a membrane protein solubilized in micelles [41]. The midpoint potentials have been accurately calculated using computational models for a helical protein with two heme *b* cofactors, suggesting that the dielectric constant and heme propionic acid groups play key roles in establishing the potentials [42].

Overall, these results on natural and *de novo* proteins show that the $E_m(Fe^{2+}/Fe^{3+})$ of hemes are influenced by not only the chemical nature of the heme substitutents, but also protein interactions. A primary influence is the nature of the axial coordination to the central heme iron but equally important to the midpoint potentials are electrostatic interactions and the dielectric nature of the protein environment. The availability of *de novo* proteins with heme cofactors is providing the opportunity to investigate the effect of protein interactions with a flexibility not available in natural proteins.

2.3. Midpoint potential of P865

In *Rb. sphaeroides*, the primary electron donor, P865, is a pair of coupled BChls that overlap at the ring A position with a separation of ~3 Å (Fig. 4) [43–47]. The central magnesium of each tetrapyrrole macrocycle is coordinated by a His, L173 and M202 to the A and B sides of P865, respectively (Fig. 4). Light excitation results in an efficient transfer of an electron from P865* through a series of electron acceptors to form the charge-separated state $P865^{\bullet+}Q_B^{\bullet-}$. The ability of P865 to serve as the primary electron donor is determined by $E_m(P865/P865^{\bullet+})$ and the potentials of the electron acceptors. For wild-type reaction centers, $E_m(P865/P865^{\bullet+})$ has been measured to be 0.505 V [48–51]. The BChl monomers and Bphe monomers are buried in the protein and are not accessible to chemical or electrochemical titrations, hence their midpoint potentials have not been experimentally established. However, based upon spectroscopic measurements of the initial electron transfer, the difference in potentials between P865 and the bacteriopheophytin acceptor results in a ~0.2 eV energy difference relative to the energy of P865* that serves as the driving force for the forward electron transfer [52,53].

The BChl cofactors have several distinctive properties compared to hemes. The central metal is magnesium in BChl rather than iron as found in heme. In contrast to the redox reactions being considered to occur at the iron in hemes, the electrons of BChls are highly distributed along the macrocycle and the molecular orbitals of the electrons reflect the properties of the entire cofactor. While the metals in both BChls and hemes have four planar nitrogen ligands, BChl is found to have only one axial ligand rather than two as found for hemes. The

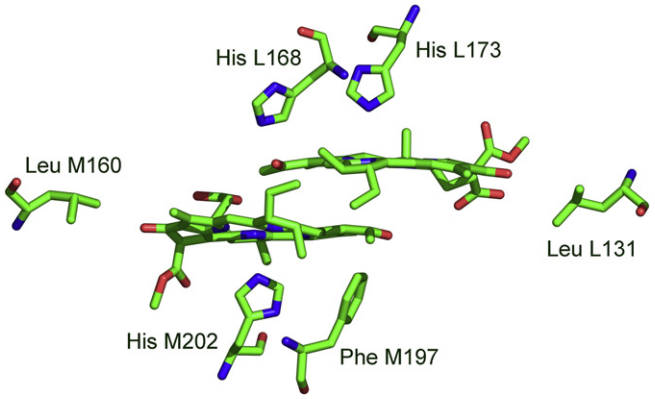

Fig. 4. Three-dimensional structure of the bacteriochlorophyll dimer, P865, from *Rb. sphaeroides*. Two BChls are in close contact with the central Mg coordinated by His L173 and M202 with a hydrogen bond to His L168 (color coded by atom type). Also shown are nearby residues Leu L131, Leu M160, and Phe M197 that when altered to His form a hydrogen bond to P865. Coordinates from Allen and coworkers [43] (4RCR).

effects of modifications of the axial ligands on E_m(P865/P865•$^+$) are difficult to determine. Alteration of the single protein ligand can lead to loss of active protein or in some cases result in a heterodimer donor, with one BChl and one bacteriopheophytin [54]. Alternatively, substitution of one of the coordinating ligands to P865, His M202, to Gly apparently resulted in incorporation of water as a ligand with no change in E_m(P865/P865•$^+$) suggesting only a weak dependence of the potential on the axial ligand [55].

Due to the highly delocalized nature of the electron orbitals in BChls, the energies of these orbitals are sensitive to interactions with neighboring cofactors. In reaction centers, the two BChls forming P865 are close together (Fig. 4) and the electrons are delocalized over both macrocycles. This effect on the electronic properties of P865 can be described using a Hückel molecular orbital model [54,56–60]. In this model, the two BChls are coupled together according to the coupling parameter β but are energetically inequivalent with energies of ε_A and ε_B. The model predicts that the observed E_m(P865/P865•$^+$) is related to the relative amount of the unpaired electron density over the A-side and B-side BChls, ρ_A/ρ_B, as given by

$$E_m\left(P865/P865^{\bullet+}\right) = -\epsilon_B - \beta\sqrt{\rho_A/\rho_B} \quad (8)$$

The Hückel model can be used qualitatively to explain the effects of protein interactions on the value of E_m(P865/P865•$^+$). Electrostatic interactions primarily alter the energetics as measured by ε_A and ε_B. In wild-type reaction centers, the energy of the B-side BChl is lower than that of the A side BChl of P865 (Fig. 5). The value of E_m(P865/P865•$^+$) will increase or decrease as the BChls of P865 are energetically stabilized or de-stabilized, respectively. Placing or removing ionizable residues at several different positions located approximately 10 to 15 Å from P865 changes the potential depending on the sign of the charge [7,9,61]. For example, the introduction of Asp in place of Asn M199 decreases E_m(P865/P865•$^+$) by 0.07 V as the pH increases to 9.5 due to the added electrostatic interaction with Asp M199 [7].

The E_m(P865/P865•$^+$) can be systematically manipulated by altering the number of hydrogen bonds between the protein and the two BChls forming P865. BChl *a* has two positions, at the acetyl group of ring A and the keto carbonyl of ring E, that are part of the conjugated macrocycle and can serve as proton acceptors. Wild-type reaction centers have one hydrogen bond between His L168 and the acetyl group of the A side of P865 (Fig. 4). Placing a His at L131, M160, or M197 resulted in the addition of a hydrogen bond to the conjugated system of P865. By constructing mutants with different combinations of these alterations, the number of hydrogen bonds was decreased to zero or increased to four. Removing the existing bond resulted in a 0.09 V decrease in E_m(P865/P865•$^+$) while adding a bond at one of the other positions resulted in a 0.06–0.12 V increase in the midpoint potential [49,51,62,63]. The measured change in E_m(P865/P865•$^+$) was found to be additive with the number of hydrogen bonds, with the presence of three additional bonds, and thus a total of four bonds, resulting in an increase of 0.26 V compared to wild type [51].

In addition to altering E_m(P865/P865•$^+$), changes in the hydrogen bond interactions affect the electron spin distribution over P865. The addition of a hydrogen bond to the BChl near M160 stabilizes the B-side BChl, making the energies of the two halves more asymmetric and resulting in a larger ρ_A/ρ_B ratio (Fig. 5). The addition of a hydrogen bond to the BChl near L131 has the opposite effect as it makes the dimer more symmetric and hence brings the ratio to near unity. In both cases stabilization by the addition of the hydrogen bonds results in a higher value of E_m(P865/P865•$^+$), that is, a larger amount of energy is required to remove an electron from P865 to the continuum. The model can also quantitatively describe these changes although some additional parameters, such as the reorganization energy associated with moving a charge over P865, must be included for an accurate modeling of the electronic structure of P865 [58,60].

Thus, E_m(P865/P865•$^+$) is influenced by a number of interactions. The primary determinant is the coupling between the BChls of P865 due to the delocalization of electrons over the two macrocycles. In contrast to hemes, the impact of changes of the magnesium coordination on E_m(P865/P865•$^+$) appears to be small as has also been found for the midpoint potential of P680, E_m(P680/P680•$^+$) [55,64,65]. Electrostatic interactions and hydrogen-bonding interactions alter E_m(P865/P865•$^+$) by changing the energies of the molecular orbitals. The additive nature of the effects of the hydrogen bonds can result in a large E_m(P865/P865•$^+$) change compared to wild type with the presence of four hydrogen bonds resulting in a highly oxidizing P865.

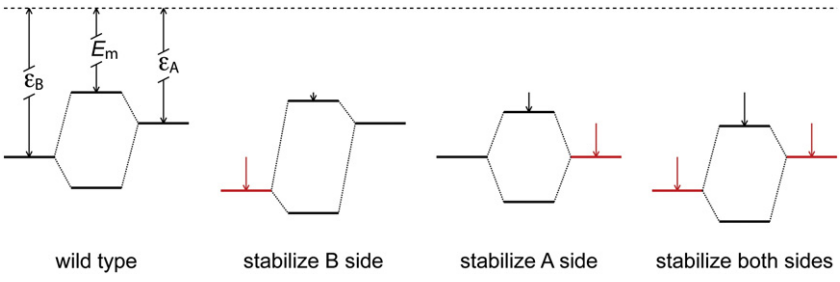

Fig. 5. Hückel model of P865. In wild type, the molecular orbitals are split by the inequivalence in the energies of the BChls on the A side and B side, identified as ε_A and ε_B, and their coupling according to Eq. (8). The E_m value of P865/P865•$^+$ corresponds to the energy difference between the highest molecular orbital and the continuum. The stabilization of the energy of the BChl on the B side of P865, by a change in the protein interactions such as the introduction of a hydrogen bond to the B side of P865, results in a larger E_m value and a more asymmetric dimer. The stabilization of the BChl on the A side of P865 also results in a larger E_m value but a more symmetric dimer. The results are additive with the stabilization of both sides resulting in a much larger change in E_m with the symmetry of the dimer remaining unchanged.

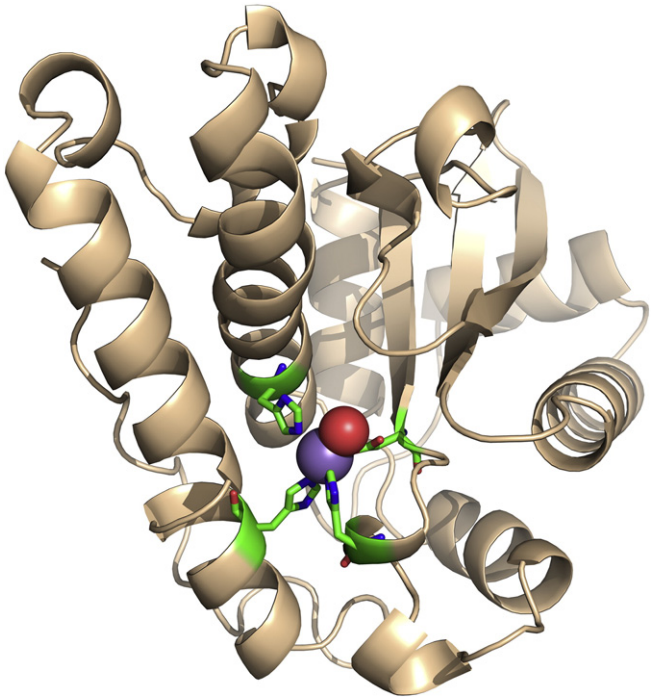

Fig. 6. Three-dimensional structure of Mn-superoxide dismutase from *E. coli*. The structure shows an overall globular fold (wheat) surrounding the central Mn-cofactor coordinated by His 26, His 81, Asp 167, His 171, and a hydroxide molecule (colored by atom type). Coordinates from Edwards and coworkers [68]) (1VEW).

2.4. Midpoint potentials of Mn-cofactors

One of the most common redox-active metals found in proteins is manganese [66]. Manganese cofactors in proteins are typically found as metal clusters coordinated by a combination of carboxylates, histidines, and water molecules. The best-characterized Mn-containing enzyme is Mn-superoxide dismutase that has a mononuclear Mn-cofactor and catalyzes the conversion of superoxide into molecular oxygen and hydrogen peroxide [67]. The Mn-cofactor of Mn-superoxide dismutase from *Escherichia coli* is coordinated by three His (26, 81, 171), Asp 167, and a hydroxide molecule [68] (Fig. 6). Mn-superoxide dismutase performs two redox reactions in which the oxidation state of the Mn-cofactor cycles between the 2+ and 3+ states. In one of the redox reactions, the conversion of superoxide into molecular oxygen is coupled with the reduction of the manganese. In the other redox reaction, the conversion of superoxide into hydrogen peroxide is coupled with the oxidation of the manganese. The midpoint potential of the Mn-cofactor, $E_m(Mn^{2+}/Mn^{3+})$, is between 0.29 and 0.39 V depending upon the source of the enzyme, and is poised between the potentials of −0.16 V and +0.89 V associated with the two reactions [67].

The Mn-superoxide dismutases have a strong structural homology with Fe-superoxide dismutases, including the same metal coordination to three His, one Asp, and one solvent molecule. The midpoint potential measured for Fe-superoxide dismutases is 0.22 V, which is lower than the 0.29–0.39 V potential measured for Mn-superoxide dismutase. Biochemically replacing the Fe with Mn increases the midpoint potential to over 0.96 V primarily due to the intrinsically higher potential associated with Mn compared to Fe. Also contributing are a series of small changes in the interactions with the surrounding protein, including hydrogen bond interactions with one of the metal ligands, a bound water [69,70].

Experimental determination of the midpoint potentials of Mn-cofactors in proteins has been restricted due to a variety of factors, such as poor equilibration of the Mn-cofactor with the electrodes that required use of long times for accurate measurements [71]. In some cases, Mn-cofactors can be poised in different oxidation states. For example, the enzyme Mn-peroxidase is a major factor in the lignin-degrading metabolism of fungi and contains a redox active mononuclear Mn-cofactor that is coordinated by two water ligands and four carboxylates, one of which is a heme propionate [72]. Despite a considerable amount of spectroscopic studies, determination of the $E_m(Mn^{2+}/Mn^{3+})$ has been difficult [73]. Likewise, the enzyme Mn-catalase, which facilitates the disproportionation of hydrogen peroxide into water and molecular oxygen using a dinuclear Mn cofactor, has been characterized in the $(Mn^{2+})_2$, $(Mn^{2+}Mn^{3+})$, and $(Mn^{3+})_2$ states by the addition of substrates such as hydrogen peroxide or hydroxylamine, although the midpoint potentials of these oxidation states have not been established [74].

The limited amount of experimental data on the midpoint potentials of Mn-cofactors in proteins makes the effect of protein interactions difficult to evaluate. However, the design of novel redox-active Mn-cofactors provides a promising future. As an example, the bacterial reaction center has been modified to gain a new redox active mononuclear Mn-cofactor [75]. The mononuclear Mn-cofactor was introduced at a site homologous to the site of the Mn_4Ca cofactor of photosystem II, approximately 10 Å from the primary electron donor P865 and coordinated by Glu M168, Glu M173, His M193, Asp M288, and a bound water molecule (Fig. 7). The Mn^{2+}/Mn^{3+} midpoint potential was determined by making use of the ability of this new cofactor to serve as a rapid electron donor to $P865^{\bullet+}$. Light excitation results in the formation of an initial charge-separated state, $P865^{\bullet+}Q_B^{\bullet-}$ followed by a subsequent electron transfer that oxidizes Mn^{2+}:

$$Mn^{2+}PQ \xrightarrow{h\nu} Mn^{2+}P^{*}Q \rightarrow Mn^{2+}P^{+}Q^{-} \overset{\Delta G^0}{\Leftrightarrow} Mn^{3+}PQ^{-} \quad (9)$$

The amount of Mn^{3+} produced is dependent upon the free energy difference ΔG° for the last step. Using Eq. (3), ΔG° can be expressed in terms of the difference in the midpoint potential for Mn, $E_m(Mn^{2+}/Mn^{3+})$ and the midpoint potential for P865, $E_m(P865/P865^{\bullet+})$:

$$\Delta G^{\circ} = F\left[E_m\left(Mn^{2+}/Mn^{3+}\right) - E_m\left(P865/P865^{\bullet+}\right)\right] \quad (10)$$

The ability of the Mn cofactor to transfer an electron to $P865^{\bullet+}$ was examined in a series of mutants that had altered $E_m(P865/P865^{\bullet+})$ values [76]. For each mutant the relative amount of $P865^{\bullet+}$ compared to P865 was determined using optical spectroscopy, allowing an estimation of the relative amounts of Mn^{2+} and Mn^{3+}. For example, at relatively low $E_m(P865/P865^{\bullet+})$ values the spectrum showed only the P865 state indicating no oxidation by the Mn-cofactor while at higher $E_m(P865/P865^{\bullet+})$ values the P865 state was completely absent indicating full oxidation of the Mn-cofactor. By fitting this dependence to a modified Nernst equation a $E_m(Mn^{2+}/Mn^{3+})$ of 0.625 V was determined [76].

The $E_m(Mn^{2+}/Mn^{3+})$ of 0.625 V in the modified reaction centers poises the potential at a value comparable to the $E_m(Mn^{2+}/Mn^{3+})$ of Mn-superoxide dismutase and between the potentials needed for oxidation of superoxide into molecular oxygen and reduction of superoxide into hydrogen peroxide. To test the ability of the Mn-cofactor of the modified reaction centers to perform such reactions, the modified reaction centers were exposed to superoxide [77]. The Mn-cofactor was found to be capable of oxidizing superoxide into molecular oxygen. The modified reaction centers did not reduce superoxide as performed by Mn-superoxide dismutase, presumably due to an inability to couple that reaction with the needed transfer of protons. However, by using light to excite P865 and subsequently oxidize the Mn^{2+} to Mn^{3+}, the system could cycle between the Mn^{2+} to Mn^{3+} states in the presence of superoxide and light. This activity had a relatively high efficiency with a k_{cat} of approximately 1 s^{-1} that is significantly larger than typically observed for designed enzymes, and a K_M of 35–40 μM that is comparable to the value of 50 μM for Mn-superoxide dismutase.

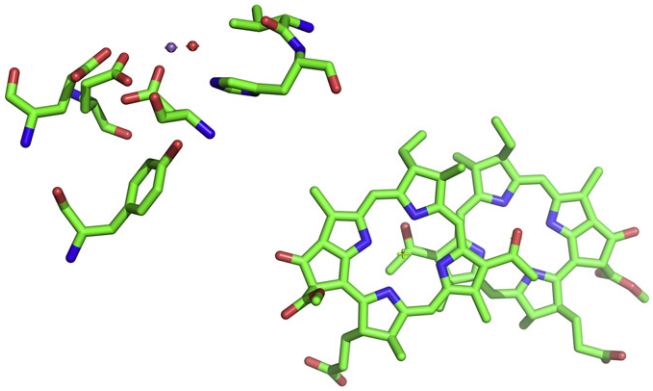

Fig. 7. Three-dimensional structure of the Mn-cofactor in modified reaction centers from *Rb. sphaeroides*. The structure shows the mononuclear Mn-cofactor (purple sphere) with the amino acid residues forming the binding site, Tyr M164, Glu M168, Glu M173, Val M192, His M193, and Asp 288 and P865 (colored by atom type). Coordinates are from Thielges and coworkers [75] (1Z9J).

3. Implications for water oxidation

One of the outstanding redox questions in biological systems is how water oxidation proceeds in photosystem II [3]. Water oxidation is a complex four-electron redox reaction that produces no stable intermediates. The site of water oxidation is the Mn_4Ca cluster of photosystem II that is located approximately 10 Å from the primary electron donor of photosystem II, P680, with Y_Z serving as a bridging cofactor (Fig. 8) [78–82]. The Mn_4Ca cluster has a distorted cubane configuration and is coordinated by several carboxylates, histidines, and four bound water molecules. Water oxidation proceeds through the sequential transfer of electrons from the Mn_4Ca cluster, which becomes systematically oxidized during the S cycle. In order to oxidize water, both P680 and the Mn_4Ca cluster must have midpoint potentials of at least +0.82 V at pH 7 and +0.93 at pH 5, which is the pH range of the thylakoid lumen. Because the energetics associated with water oxidation lie near or above the midpoint potential of water, they cannot be directly experimentally measured.

The value of E_m(P680/P680$^{\bullet+}$) is estimated to be 1.1–1.3 V based upon the electron transfer rates involving P680 [17–20]. The midpoint potential of chlorophylls (Chls) in solution are strongly dependent upon the solvent, with 0.81 V in acetonitrile being a typical value [83]. Electrostatic interactions between P680 and the protein environment are thought to be primarily responsible for the increase of 0.3–0.5 V for E_m(P680/P680$^{\bullet+}$) compared to the potential of isolated Chl [10,84]. The spin density ratio measured for P680$^{\bullet+}$ is 4:1, indicating that the majority of the unpaired spin resides on one of the Chls forming P680 [85–87]. Using the Hückel model (Fig. 5), this ratio is consistent with an inequivalence in the energies of the Chls. Electrostatic calculations have estimated the difference in the energies of the Chls to be 0.1 V [88]. The spin density ratio of P680$^{\bullet+}$ reflects the asymmetry in electrostatic interactions between P680 and several conserved D1/D2 pairs (Asn D1-181/Arg D2-180, Asn D1-298/Arg D2-294, Asp D1-61/His D2-61, Glu D1-189/Phe D2-188, and Asp D1-170/Phe D2-169) [88]. Although hydrogen bonds have been used to increase E_m(P865/P865$^{\bullet+}$), the lack of any hydrogen bonds to P680 in the three-dimensional structure shows that these interactions do not contribute to the high value of E_m(P680/P680$^{\bullet+}$) [82]. The dielectric properties of the protein surrounding P865 and P680 are thought to be similar, and so the electrostatic contributions to the significantly larger value of E_m(P680/P680$^{\bullet+}$) compared to E_m(P865/P865$^{\bullet+}$) arise from multiple interactions with specific residues and cofactors [10,84].

Several questions remain about the oxidation states of the Mn_4Ca cluster during the S cycles as there are no direct electrochemical measurements of any state. Based upon spectroscopic measurements, the S_0 and S_2 states are most likely in the ($3Mn^{3+}Mn^{4+}$) and ($Mn^{3+}3Mn^{4+}$)

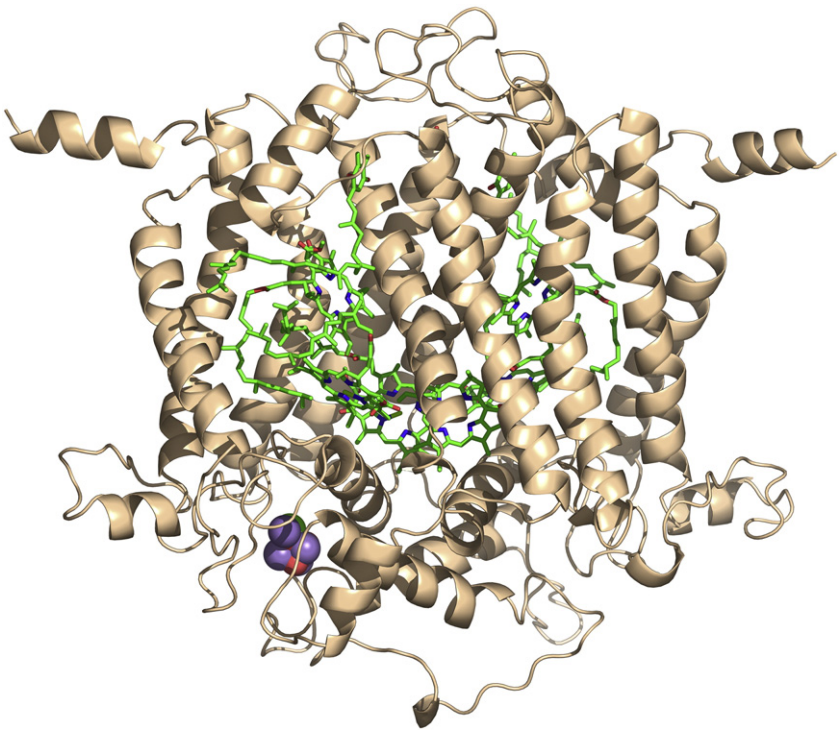

Fig. 8. Three-dimensional structure of photosystem II from *Th. elongatus*. The structure shows the two core subunits, D1 and D2 (wheat), and the core cofactors, including the Mn_4Ca cluster (colored by atom type). Coordinates from Ferreira and coworkers [79] (1S5L).

states, respectively [89,90]. Whether the Mn_4Ca cluster is oxidized during the S2 to S3 transition is debated, although electron paramagnetic resonance spectroscopy is consistent with manganese oxidation. Consequently, the crucial S_4 state most likely includes a Mn^{5+} or Mn^{4+}-oxyl radical contribution. The energetics of the S cycle transitions have been inferred based upon the associated electron transfer rates yielding estimates of ~1.1 V for the midpoint potentials of the S1/S2 and S2/S3 redox couples [20]. The earlier S states are thought to have lower potentials, in part to avoid unfavorable reactions such as production of hydrogen peroxide, with the later states becoming more oxidizing. While synthetic Mn_4 compounds can support highly oxidizing states, oxidation of the Mn_4Ca cluster is coupled with proton transfer involving Y_Z resulting in a leveling of potentials through the S cycles [19,90]. Compared to the 0.6 V potential measured for the Mn-cofactor in modified reaction centers, the higher potentials of the Mn_4Ca cluster are consistent with metal clusters undergoing transitions from more oxidized states rather than a simple Mn^{2+} to Mn^{3+} redox reaction [90].

The factors controlling the redox potentials of P680 and the Mn_4Ca cluster continue to be investigated as such parameters are key in understanding the water oxidation mechanism. The availability of the three-dimensional structure of photosystem II provides the opportunity to perform calculations to estimate the relative contributions of factors such as electrostatic interactions, the local dielectric constant, and other effects arising due to the protein environment. In principle, the highly-oxidizing bacterial reaction centers have the chemical capability but require a Mn cluster capable of storing the four equivalents; research is underway to develop reaction centers with a multinuclear Mn-cluster capable of performing multi-electron redox reactions. Meanwhile, extensive spectroscopic measurements of photosystem II are leading to a better understanding of the different S states [89,91]. Together, the continuing efforts to probe the factors that control water oxidation should yield general insight into the mechanisms of complex redox reactions in biological systems.

Acknowledgements

We acknowledge support from a grant from the National Science Foundation, CHE 1158552.

References

[1] R.E. Blankenship, M.T. Madigan, C.E. Bauer (Eds.), Anoxygenic Photosynthetic Bacteria, Kluwer, Dordrecht, 1995.
[2] C.N. Hunter, F. Daldal, M.C. Thurnauer, J.T. Beatty (Eds.), The Purple Phototrophic Bacteria, Springer Dordrecht, Heidelberg, 2009.
[3] T.J. Wydrzynski, K. Satoh (Eds.), Photosystem II: The Light-induced Water:Plastoquinone Oxidoreductase, Springer-Verlag Publishers, Dordrecht, 2005.
[4] J.C. Williams, J.P. Allen, Directed modification of reaction centers from purple bacteria, in: C.N. Hunter, F. Daldal, M.C. Thurnauer, J.T. Beatty (Eds.), The Purple Phototrophic Bacteria, Kluwer, Dordrecht, 2009, pp. 337–353.
[5] P. Maroti, D.K. Hanson, L. Baciou, M. Schiffer, P. Sebban, Proton conduction within reaction centers of *Rhodobacter capsulatus*: the electrostatic role of the protein, Proc. Natl. Acad. Sci. U. S. A. 91 (1994) 5617–5621.
[6] A. Ivancich, T.A. Mattioli, K. Artz, S. Wang, J.P. Allen, J.C. Williams, Influence of Asn/His L166 on the hydrogen-bonding pattern and redox potential of the primary donor of purple bacterial reaction centers, Biochemistry 36 (1997) 3027–3036.
[7] J.C. Williams, A.L.M. Haffa, J.L. McCulley, N.W. Woodbury, J.P. Allen, Electrostatic interactions between charged amino acid residues and the bacteriochlorophyll dimer in reaction centers from *Rhodobacter sphaeroides*, Biochemistry 40 (2001) 15403–15407.
[8] M.R. Gunner, B. Honig, Electrostatic control of the midpoint potentials in the cytochrome subunit of the *Rhodopseudomonas viridis* reaction center, Proc. Natl. Acad. Sci. U. S. A. 88 (1991) 9151–9155.
[9] E.T. Johnson, W.W. Parson, Electrostatic interactions in an integral membrane protein, Biochemistry 41 (2002) 6483–6494.
[10] H. Ishikita, W. Saenger, J. Biesiadka, B. Loll, E.W. Knapp, How photosynthetic reaction centers control oxidation power in chlorophyll pairs P680, P700, and P870, Proc. Natl. Acad. Sci. U. S. A. 26 (2006) 9855–9860.
[11] E. Bombarda, G.M. Ulmann, Continuum electrostatic investigations of charge transfer processes in biological molecules using a microstate description, Faraday Discuss. 148 (2011) 173–193.
[12] F.A. Armstrong, H.A.O. Hill, N.J. Walton, Direct electrochemistry of redox proteins, Acc. Chem. Res. 21 (1988) 407–413.
[13] A.J. Bard, L.R. Faulkner, Electrochemical Methods, John Wiley, NY, 2001.
[14] Y. Zhang, A.M. LaFountain, N. Magdaong, M. Fuciman, J.P. Allen, H.A. Frank, J.F. Rusling, Thin film voltammetry of wild type and mutant reaction center proteins from photosynthetic bacteria, J. Phys. Chem. B 115 (2011) 3226–3232.
[15] P.L. Dutton, K.M. Petty, H.S. Bonner, S.D. Morse, Cytochrome c_2 and reaction center of *Rhodopseudomonas spheroides* Ga. Membranes, extinction coefficients, content, half-reduction potentials, kinetics and electric field alterations, Biochim. Biophys. Acta 387 (1975) 536–556.
[16] P.L. Dutton, Redox potentiometry: determination of midpoint potentials of oxidation-reduction components of biological electron-transfer systems, Methods Enzymol. 54 (1978) 411–435.
[17] V.V. Klimov, S.I. Allakhverdiev, S. Demeter, A.A. Krasnovskii, Photoreduction of pheophytin in photosystem 2 of chloroplasts with respect to redox potential of the medium, Dokl. Akad. Nauk SSSR 249 (1979) 227–230.
[18] I. Vass, S. Styring, pH-dependent charge equilibria between tyrosine-D and the S states in photosystem II: estimation of relative midpoint redox potentials, Biochemistry 30 (1991) 830–839.
[19] C. Tommos, G.T. Babcock, Proton and hydrogen currents in photosynthetic water oxidation, Biochim. Biophys. Acta 1458 (2000) 199–219.
[20] F. Rappaport, B.A. Diner, Primary photochemistry and energetics leading to the oxidation of the $(Mn)_4Ca$ cluster and to the evolution of molecular oxygen in photosystem II, Coord. Chem. Rev. 252 (2008) 259–272.
[21] G.R. Moore, G.W. Pettigrew, Cytochromes *c* evolutionary, structural and physicochemical aspects, Springer-Verlag, NY, 1990.
[22] L.J. Smith, A. Kahraman, J.M. Thornton, Heme proteins—diversity in structural characteristics, function, and folding, Proteins 78 (2010) 2349–2368.
[23] T. Takano, R.E. Dickerson, Redox conformation changes in refined tuna cytochrome *c*, Proc. Natl. Acad. Sci. U. S. A. 77 (1980) 6371–6375.
[24] H.L. Axelrod, G. Feher, J.P. Allen, A.J. Chirino, M.W. Day, B.T. Hsu, D.C. Rees, Crystallization and X-ray structure determination of cytochrome c_2 from *Rhodobacter sphaeroides* in three crystal forms, Acta Crystallogr. D 50 (1994) 596–602.
[25] C.J.A. Wallace, I. Clark-Lewis, Functional-role of heme ligation in cytochrome *c*—effects of replacement of methionine-80 with natural and nonnatural residues by semisynthesis, J. Biol. Chem. 267 (1992) 3852–3861.
[26] Z. Zheng, M.R. Gunner, Analysis of the electrochemistry of hemes with E(m)s spanning 800 mV, Proteins 75 (2009) 719–734.
[27] X. Lin, J.C. Williams, J.P. Allen, P. Mathis, Relationship between rate and free energy difference from electron transfer from cytchrome c_2 to the reaction center from *Rhodobacter sphaeroides*, Biochemistry 33 (1994) 13517–13523.
[28] E.A. Berry, D.W. Lee, L.S. Huang, F. Daldal, Structural and mutational studies of the cytochrome bc_1, in: C.N. Hunter, F. Daldal, M.C. Thurnauer, J.T. Beatty (Eds.), The Purple Phototrophic Bacteria, Kluwer, Dordrecht, 2009, pp. 425–450.
[29] W. Nitschke, S.M. Dracheva, Reaction center associated cytochromes, in: R.E. Blankenship, M.T. Madigan, C.E. Bauer (Eds.), Anoxygenic Photosynthetic Bacteria, Kluwer, Dordrecht, 1995, pp. 775–805.
[30] J. Deisenhofer, O. Epp, I. Sinning, H. Michel, Crystallographic refinement at 2.3 Å resolution and refined model of the photosynthetic reaction centre from *Rhodopseudomonas viridis*, J. Mol. Biol. 246 (1995) 429–457.
[31] S.M. Dracheva, L.A. Drachev, A.A. Konstantinov, A.Y. Smenov, V.P. Skulacheva, A.M. Arutjunjan, V.A. Shuvalov, S.M. Zaberezhnaya, Electrogenic steps in the redox reactions catalyzed by photosynthetic reaction centre complex from *Rhodopseudomonas viridis*, Eur. J. Biochem. 171 (1988) 253–264.
[32] W. Nitchke, A.W. Rutherford, Tetraheme cytochrome *c* subunit of *Rhodopseudomonas viridis* characterized by EPR, Biochemistry 28 (1989) 3161–3168.
[33] D.E. Robertson, R.S. Farid, C.C. Moser, J.L. Urbauer, S.E. Mulholland, R. Pidikiti, J.D. Lear, A.J. Wand, W.F. DeGrado, P.L. Dutton, Design and synthesis of multi-haem proteins, Nature 368 (1994) 425–432.
[34] W.F. DeGrado, C.M. Summa, V. Pavone, F. Nastri, A. Lombardi, *De novo* design and structural characterization of proteins and metalloproteins, Annu. Rev. Biochem. 68 (1999) 779–819.
[35] Y. Lu, S.M. Berry, T.D. Pfister, Engineering novel metalloproteins: design of metal-binding sites into native protein scaffolds, Chem. Rev. 101 (2001) 3047–3080.
[36] C.J. Reedy, B.R. Gibney, Heme protein assemblies, Chem. Rev. 104 (2004) 617–649.
[37] D. Ghosh, V.L. Pecoraro, Probing metal–protein interactions using a *de novo* design approach, Curr. Opin. Chem. Biol. 9 (2005) 97–103.
[38] S.J. Lahr, D.E. Engel, S.E. Stayrook, O. Maglio, B. North, S. Geremia, A. Lombardi, W.F. DeGrado, Analysis and design of turns in alpha-helical hairpins, J. Mol. Biol. 246 (2005) 1441–1454.
[39] H.K. Privett, C.J. Reedy, M.L. Kennedy, B.R. Gibney, Non-natural amino acid ligands in heme protein design, J. Am. Chem. Soc. 124 (2002) 6828–6829.
[40] M.L. Kennedy, B.R. Gibney, Metalloprotein and redox protein design, Curr. Opin. Struct. Biol. 11 (2001) 485–490.
[41] J.M. Cordova, P.L. Noack, S.A. Hilcove, J.D. Lear, G. Ghirlanda, Design of a functional membrane protein by engineering a heme-binding site in glycophorin A, J. Am. Chem. Soc. 129 (2007) 512–518.
[42] A.P. Gamiz-Hernandez, G. Kieseritzky, A.S. Galstyan, O. Demir-Kavuk, E.-W. Knapp, Understanding properties of cofactors in proteins: redox potentials of synthetic cytochromes *b*, ChemPhysChem 11 (2010) 1196–1206.
[43] J.P. Allen, G. Feher, T.O. Yeates, H. Komiya, D.C. Rees, Structure of the reaction center from *Rhodobacter sphaeroides* R-26: the cofactors, Proc. Natl. Acad. Sci. U. S. A. 84 (1987) 5730–5734.
[44] C.H. Chang, O. El-Kabbani, D. Tiede, J. Norris, M. Schiffer, Structure of the membrane-bound protein photosynthetic reaction center from *Rhodobacter sphaeroides*, Biochemistry 30 (1991) 5352–5360.

[45] U. Ermler, G. Fritzsch, S.K. Buchanan, H. Michel, Structure of the photosynthetic reaction centre from *Rhodobacter sphaeroides* at 2.65 Å resolution: cofactors and protein–cofactor interactions, Structure 2 (1994) 925–936.
[46] K.E. McAuley, P.K. Fyfe, J.P. Ridge, N.W. Isaacs, R.J. Cogdell, M.R. Jones, Structural details of an interaction between cardiolipin and an integral membrane protein, Proc. Natl. Acad. Sci. U. S. A. 96 (1999) 14706–14711.
[47] A. Camara-Artigas, D. Brune, J.P. Allen, Interactions between lipids and bacterial reaction centers determined by protein crystallography, Proc. Natl. Acad. Sci. U. S. A. 99 (2002) 11055–11060.
[48] D.A. Moss, M. Leonhard, M. Bauscher, W. Mantele, Electrochemical redox titration of cofactors in the reaction centers from *Rhodobacter sphaeroides*, FEBS Lett. 283 (1991) 33–36.
[49] J.C. Williams, R.G. Alden, H.A. Murchison, J.M. Peloquin, N.W. Woodbury, J.P. Allen, Effects of mutations near the bacteriochlorophylls in reaction centers from *Rhodobacter sphaeroides*, Biochemistry 31 (1992) 11029–11037.
[50] V. Nagarajan, W.W. Parson, D. Davis, C.C. Schenck, Kinetics and free energy gaps of electron-transfer reactions in *Rhodobacter sphaeroides* reaction centers, Biochemistry 32 (1993) 12324–12336.
[51] X. Lin, H.A. Murchison, V. Nargaragan, W.W. Parson, J.P. Allen, J.C. Williams, Specific alteration of the oxidation potential of the electron donor in reaction centers from *Rhodobacter sphaeroides*, Proc. Natl. Acad. Sci. U. S. A. 91 (1994) 10265–10269.
[52] N.W. Woodbury, J.P. Allen, The pathway, kinetics and thermodynamics of electron transfer in wild type and mutant reaction centers of purple nonsulfur bacteria, in: R.E. Blankenship, M.T. Madigan, C.E. Bauer (Eds.), Anoxygenic Photosynthetic Bacteria, Kluwer, Dordrecht, 1995, pp. 527–557.
[53] H. Wang, S. Lin, J.P. Allen, J.C. Williams, S. Blankert, C. Laser, N.W. Woodbury, Protein dynamics control the kinetics of initial electron transfer in photosynthesis, Science 316 (2007) 747–750.
[54] J.P. Allen, J.C. Williams, Energetics of cofactors in photosynthetic complexes: Relationship between protein-cofactor interactions and midpoint potentials, in: J. Goldbeck, A. van der Est (Eds.), The Biophysics of Photosynthesis, Springer Dordrecht, in press.
[55] J.O. Goldsmith, B. King, S.G. Boxer, Mg coordination by amino acid side chains is not required for assembly and function of the special pair in bacterial photosynthetic reaction centers, Biochemistry 35 (1996) 2421–2428.
[56] M. Plato, F. Lendzian, W. Lubitz, K. Möbius, Molecular orbital study of electronic asymmetry in primary donors of bacterial reaction centers, in: J. Breton, A. Vermeglio (Eds.), The Photosynthetic Bacterial Reaction Center II: Structure, Spectroscopy, and Dynamics, Plenum, New York, 1992, pp. 109–118.
[57] J. Breton, E. Nabedryk, W.W. Parson, A new infrared electronic transition of the oxidized primary donor in bacterial reaction centers: a way to access resonance interactions between the bacteriochlorophylls, Biochemistry 31 (1992) 7503–7510.
[58] F. Müh, F. Lendzian, M. Roy, J.C. Williams, J.P. Allen, W. Lubitz, Pigment–protein interactions in bacterial reaction centers and their influence on oxidation potential and spin density distribution of the primary donor, J. Phys. Chem. B 106 (2002) 3226–3236.
[59] T.P. Treynor, S.S. Andrews, S.G. Boxer, Intervalence band Stark effect of the special pair radical cation in bacterial photosynthetic reaction centers, J. Phys. Chem. B 107 (2003) 11230–11239.
[60] J.R. Reimers, N.S. Hush, A unified description of the electrochemical, charge distribution, and spectroscopic properties of the special-pair radical cation in bacterial photosynthesis, J. Am. Chem. Soc. 126 (2004) 4132–4144.
[61] E.T. Johnson, F. Müh, E. Nabedryk, J.C. Williams, J.P. Allen, W. Lubitz, J. Breton, W.W. Parson, Electronic and vibronic coupling of the special pair of bacteriochlorophylls in photosynthetic reaction centers from wild-type and mutant strains of *Rhodobacter sphaeroides*, J. Phys. Chem. B 106 (2002) 11859–11869.
[62] J.W. Stocker, A.K.W. Taguchi, H.A. Murchison, N.W. Woodbury, S.G. Boxer, Spectroscopic and redox properties of sym1 and (M)F195H: *Rhodobacter capsulatus* reaction center symmetry mutants which affect the initial electron donor, Biochemistry 31 (1992) 10356–10362.
[63] H.A. Murchison, R.G. Alden, J.P. Allen, J.M. Peloquin, A.K.W. Taguchi, N.W. Woodbury, J.C. Williams, Mutations designed to modify the environment of the primary electron donor of the reaction center from *Rhodobacter sphaeroides*: phenylalanine to leucine at L167 and histidine to phenylalanine at L168, Biochemistry 32 (1993) 3498–3505.
[64] M. Sugiura, F. Rappaport, K. Brettel, T. Noguchi, A.W. Rutherford, A. Boussac, Site-directed mutagenesis of *Thermosynechococcus elongatus* photosystem II: the O_2-evolving enzyme lacking the redox-active tyrosine D, Biochemistry 43 (2004) 13549–13563.
[65] K. Saito, J.-R. Shen, H. Ishikita, Influence of the axial ligand on the cationic properties of the chlorophyll pair in photosystem II from *Thermosynechococcus vulcanus*, Biophys. J. 102 (2012) 2634–2640.
[66] A. Siegel, H. Siegel (Eds.), Metal Ions in Biological Systems: Manganese and its Role in Biological Processes, Marcel Dekker, New York, 2000.
[67] A.-F. Miller, Superoxide dismutases: ancient enzymes and new insights, FEBS Lett. 586 (2012) 585–595.
[68] R.A. Edwards, H.M. Baker, M.M. Whittaker, J.W. Whittaker, G.B. Jameson, E.N. Baker, Crystal structure of *Escherichia coli* superoxide dismutase at 2.1 Å resolution, J. Biol. Inorg. Chem. 3 (1998) 161–171.
[69] C.K. Vance, A.F. Miller, Novel insights into the basis for *Escherichia coli* superoxide dismutase's metal-ion specificity from Mn-substituted FeSOD and its very high E_m, Biochemistry 40 (2001) 13079–13087.
[70] E. Yikilmaz, D.W. Rodgers, A.F. Miller, The crucial importance of chemistry in the structure-function link: manipulating hydrogen bonding in iron-containing superoxide dismutase, Biochemistry 45 (2006) 1151–1161.
[71] V.J.-P. Leveque, C.K. Vance, H.S. Nick, D.N. Silverman, Redox properties of human manganese superoxide dismutase and active-site mutants, Biochemistry 40 (2001) 10586–10591.
[72] M.H. Gold, H.L. Youngs, M.D.S. Gelpke, Manganese peroxidase, in: A. Sigel, H. Sigel (Eds.), Manganese and Its Role in Biological Systems, Marcel Dekker Publishers, New York, 2000, pp. 559–586.
[73] M. Petruccioli, M. Frasconi, D. Quaratino, S. Covino, G. Favero, F. Mazzei, F. Federici, A. D'Annibale, Kinetic and redox properties of MnP II, a major manganese peroxidase isoenzyme from *Panus tigrinus* CBS 577.79, J. Biol. Inorg. Chem. 14 (2009) 1153–1163.
[74] D.W. Yoder, J. Hwang, J.E. Penner-Hahn, Manganese peroxidase, in: A. Sigel, H. Sigel (Eds.), Manganese and Its Role in Biological Systems, Marcel Dekker Publishers, New York, 2000, pp. 527–557.
[75] M.T. Thielges, G. Uyeda, A. Cámara-Artigas, L. Kálmán, J.C. Williams, J.P. Allen, Design of a redox-linked active metal site: manganese bound to bacterial reaction centers at a site resembling that of photosystem II, Biochemistry 44 (2005) 7389–7394.
[76] L. Kálmán, G. Uyeda, J.C. Williams, J.P. Allen, Energetics for oxidation of a bound manganese cofactor in modified bacterial reaction centers, Biochemistry 50 (2011) 3310–3320.
[77] J.P. Allen, T.L. Olson, P. Oyala, W.J. Lee, A. Tufts, J.C. Williams, Light-driven oxygen production from superoxide by Mn-binding bacterial reaction centers, Proc. Natl. Acad. Sci. U. S. A. 109 (2012) 2314–2318.
[78] A. Zouni, H.T. Witt, J. Kern, P. Fromme, N. Krauss, W. Saenger, P. Orth, Crystal structure of photosystem II from *Synechococcus elongatus* at 3.8 Å resolution, Nature 409 (2001) 739–743.
[79] K.N. Ferreira, T.M. Iverson, K. Maghlaui, J. Barber, S. Iwata, Architecture of the photosynthetic oxygen-evolving center, Science 303 (2004) 1831–1838.
[80] B. Loll, J. Kern, W. Saenger, A. Zouni, J. Biesiadka, Towards complete cofactor arrangement in the 3.0 Å resolution structure of photosystem II, Nature 438 (2005) 1040–1044.
[81] J. Yano, J. Kern, K. Sauer, M.J. Latimer, Y. Pushkar, J. Biesiadka, B. Loll, W. Saenger, J. Messinger, A. Zouni, V. Yachandra, Where water is oxidized to dioxygen: structure of the photosynthetic Mn_4Ca cluster, Science 314 (2006) 821–825.
[82] Y. Umena, K. Kawakami, J.R. Shen, N. Kamiya, Crystal structure of oxygen-evolving photosystem II at a resolution of 1.9 Å, Nature 473 (2011) 55–61.
[83] M. Kobayashi, S. Ohashi, K. Iwamoto, Y. Shiraiwa, Y. Kato, T. Watanabe, Redox potential of chlorophyll *d in vitro*, Biochim. Biophys. Acta 1767 (2007) 596–602.
[84] A.W. Rutherford, P. Faller, Photosystem II: evolutionary perspectives, Phil. Trans. R. Soc. Lond. B 358 (2003) 245–253.
[85] S.E.J. Rigby, J.H.A. Nugent, P.J. O'Malley, ENDOR and special triple resonance studies of chlorophyll cation radicals in photosystem 2, Biochemistry 33 (1994) 10043–10050.
[86] B.A. Diner, E. Schlodder, P.J. Nixon, W.J. Coleman, F. Rappaport, J. Lavergne, W.J.F. Vermaas, D.A. Chisholm, Site-directed mutations at D1-His198 and D2-His197 of photosystem II in *Synechocystis* PCC 6803: Sites of primary charge separation and cation and triplet stabilization, Biochemistry 40 (2001) 9265–9281.
[87] T. Okubo, T. Tomo, M. Sugiura, T. Noguchi, Perturbation of the structure of P680 and the charge distribution on its radical cation in isolated reaction center complexes of photosystem II as revealed by Fourier transform infrared spectroscopy, Biochemistry 46 (2007) 4390–4397.
[88] K. Saito, T. Ishida, M. Sugiura, K. Kawakami, Y. Umena, N. Kamiya, J.R. Shen, H. Ishikita, Distribution of the cationic state over the chlorophyll pair of the photosystem II reaction center, J. Am. Chem. Soc. 133 (2011) 14379–14388.
[89] J.P. McEvoy, G.W. Brudvig, Water-splitting chemistry of photosystem II, Chem. Rev. 106 (2006) 4455–4483.
[90] F.A. Armstrong, Why did nature choose manganese to make oxygen? Phil. Trans. R. Soc. B 363 (2008) 1263–1270.
[91] I. Rivalta, G.W. Brudvig, V.S. Batista, Oxomanganese complexes for natural and artificial photosynthesis, Curr. Opin. Chem. Biol. 16 (2012) 11–18.